Controlling the formation and stability of ultra-thin nickel silicides - an alloying strategy for preventing agglomeration

F.A. Geenen[a], K. van Stiphout[b], A. Nanakoudis[c], S. Bals[c], A. Vantomme[b], J. Jordan-Sweet[d], C. Lavoie[d], C. Detavernier[a]

[a] *Department of Solid-State Sciences, Ghent University, 9000 Gent, Belgium*
[b] *Instituut voor Kern- en Stralingsfysica, KU Leuven, B-3001 Leuven, Belgium*
[c] *EMAT, University of Antwerp, Groenenborgerlaan 171, B-2020 Antwerp, Belgium*
[d] *IBM T.J. Watson Research Center, Yorktown Heights, NY, USA*

Abstract

The electrical contact of the source and drain regions in state-of-the-art CMOS transistors is nowadays facilitated through NiSi, which is often alloyed with Pt in order to avoid morphological agglomeration of the silicide film. However, the solid-state reaction between as-deposited Ni and the Si substrate exhibits a peculiar change for as-deposited Ni films thinner than a critical thickness of t_c=5 nm. Whereas thicker films form polycrystalline NiSi upon annealing above 450 °C, thinner films form epitaxial $NiSi_2$ films which exhibit a high resistance towards agglomeration. For industrial applications, it is therefore of utmost importance to assess the critical thickness with high certainty and find novel methodologies to either increase or decrease its value, depending on the aimed silicide formation. This paper investigates Ni films between 0 and 15 nm initial thickness by using of 'thickness gradients', which provide semi-continuous information on silicide formation and stability as a function of as-deposited layer thickness. The alloying of these Ni layers with 10 % Al, Co, Ge, Pd or Pt renders a significant change in the phase sequence as a function of thickness and dependent on the alloying element. The addition of these ternary impurities therefore change the critical thickness t_c. The results are discussed in the framework of

Email address: christophe.detavernier@ugent.be (C. Detavernier)

classical nucleation theory.

Keywords: nickel silicide, epitaxy, axiotaxy, texture

1. Introduction

Metal silicides are used in micro-electronics to establish low-resistance contacts to the source and drain regions of Si-based transistors. The currently preferred material, NiSi, exhibits limited morphological stability and suffers from significant agglomeration upon annealing (e.g. $> 500\,^{\circ}\mathrm{C}$) [1, 2, 3, 4]. Moreover, NiSi transforms into $NiSi_2$ at higher temperature (e.g. $> 700\,^{\circ}\mathrm{C}$), inducing significant change in silicon consumption and electrical properties such as contact resistance and sheet resistivity. The addition of small amounts of Pt (e.g. 10 at.%) is currently being used to delay both the agglomeration process and high-temperature $NiSi_2$ transformation [5]. Because agglomeration is driven by surface and interface energy, it is significantly more difficult to avoid for thinner silicide films. [6, 7]. This can partly be compensated by incorporating a higher Pt concentration, but this results in a higher parasitic resistivity and only delays agglomeration instead of completely stabilising the morphology. Therefore, there is an ongoing interest in alternative contact materials with improved morphological stability, for such thin (e.g. $< 10\,\mathrm{nm}$) layers.

Pioneering work by Tung *et al.* [8] demonstrated that the deposition of sub-10 nm thin Ni films onto Si substrates can result in a completely different silicide phase sequence, which forms epitaxial $NiSi_2$ instead of NiSi at low temperature. Recently, the effect of this ultrathin phase formation has regained interest [9, 10, 11], as the industry is evolving towards sub-10 nm silicide thicknesses. These studies indicate that there exists a well-defined boundary between the '*regular*' regime - where reaction of e.g. 10 nm Ni at $450\,^{\circ}\mathrm{C}$ is known to result in a polycrystalline NiSi film with axiotaxial texture - and the '*ultrathin*' regime - where reaction of e.g. 3 nm Ni at similar temperatures results in the formation of an epitaxial $NiSi_2$ layer. De Keyser *et al.* [9] showed that the ultrathin phase regime (i.e. below the critical thickness) exhibits very high morphological

stability. Knoll *et al.* [12, 13] furthermore reported on the beneficial effect of the lower Schottky barrier height of these epitaxial $NiSi_2$ films.

As the silicide contacts in the state-of-the-art micro-electronics industry are trending to sub-10 nm thickness values, it is important to determine and control the exact value of the *critical thickness* which differentiates these two phase-formation regimes. Gao *et al.* [14] recently reported on a biased-sputter-deposition strategy with pure Ni films, which increases the as-deposited mixed Ni/Si interface region and increases the maximum thickness of the formed epitaxial $NiSi_2$ films, thus increasing the critical thickness.

This paper discusses an alternative strategy based on the incorporation of ternary elements in the as-deposited film, very similar to the current approach of using Pt-alloying to enhance the performance of NiSi films. The effective value of the critical thickness t_c is determined through a methodology based on the deposition of a nickel film on a Si(001) wafers, where the nickel thickness is dependent on the position of the wafer. These deposited wafers can be used as combinatorial thickness libraries to assess t_c with high accuracy as explained in the experimental section. We studied the critical thickness for unalloyed Ni films, as well as films alloyed with 10 at % of a ternary element (i.e. Al, Co, Ge, Pd, Pt).

2. Experimental methods

Ni films were deposited on 150 mm diameter Si(001) and silicon-on-insulator (SOI) substrates through physical vapour deposition with a combinatorial approach. The thickness gradient was achieved by modulating the amount of deposited Ni with a triangular-shaped shadow mask, which resulted in a high deposition rate at one side of the substrate while almost eliminating the deposition rate at the other side of the wafer. The final deposited Ni gradient can be described as a thickness library, where the deposited Ni thickness varies quasi-linearly in the direction of the gradient as a function of the position on the substrate. The Ni content of the gradient was determined to vary from

0.5 to 15 nm equivalent thickness as determined through Rutherford backscattering spectrometry (RBS) measurements, and thus covers the thickness region of interest to study the critical thickness in the Ni-Si phase formation. This combinatorial approach is not only resource and time efficient, but also ensures that identical experimental conditions were applied for all Ni thickness values of interest.

The substrates received standard (Radio Corporation of America, RCA) chemical cleaning, ending with a 20 s dip in a 3 % HF solution prior to loading into the vacuum chamber. Sputter deposition was performed in an Ar atmosphere of 5×10^{-3} mbar, after first reaching a background pressure of 6×10^{-7} mbar. The Ni thickness gradient was optionally alloyed with 10 ± 2 at.% Al, Co or Pt by co-sputtering. This was obtained through a second shadow mask for the alloy which resulted in a constant ratio between the Ni and alloy signals as verified through X-Ray Fluorescence (Co, Pt) and RBS (Al) along the thickness gradient. Ni films with 10 at.% of Pd and Ge were also deposited with discrete equivalent Ni thicknesses (i.e. without thickness gradient) of 2, 3, 6 and 9 nm and are discussed supplementary to the gradient datasets.

These unalloyed and alloyed thickness gradients are compared as function of their Ni content. The alloying species are added in *addition* to the original Ni thickness gradient, and therefore the total thickness of the as-deposited layer is higher for the alloyed films. As Co and Pt (and Pd) are known to replace Ni atoms during silicide formation, the addition of these alloying elements render an effective increase in the metal supply to form $Ni_xM_ySi_z$ (M = Co, Pt, Pd) alloys. Other papers therefore prefer to keep the as-deposited total metal supply constant by reducing the Ni content when adding an alloying species. Such approach is not easily translated to Al (or Ge) alloying, which is known to replace the Si atoms during silicide formation. For conciseness, the amount of nickel present at every position on each gradient will be referred to by using the *equivalent* Ni thickness of the gradient, i.e. the as-deposited Ni thickness which would be measured when no alloy would be added to the layer.

The thickness library was then used in two complementary experimental ap-

proaches. In a first approach, a 150 mm long strip from the thickness library was annealed up to a specific temperature and its properties were characterised after quenching as a function of position within the library (i.e. as a function of as-deposited Ni thickness). *Ex situ* techniques were used, such as scanning electron microscopy (SEM) to evaluate layer morphology, pole-figure measurements to investigate crystalline phase, and texture and transmission electron microscopy (TEM) to assess roughness and local composition. In a second approach, a 150 mm long thickness gradient strip was cut into 15 smaller pieces of ~ 10 mm, resulting in a set of discrete samples with an average thickness difference of 1 nm. Subsequently, these individual samples were studied with *in situ* techniques, which consisted of a continuous acquisition of the sheet resistance (SR) and X-ray diffraction (XRD) during annealing. To enable a straightforward comparison in the measurements acquired both *in situ* during annealing, and *ex situ* after annealing, we used the same annealing conditions.

In situ XRD was used to monitor the solid-state reaction as a function of temperature and was performed at the X20C beamline of the National Synchrotron Light Source (NSLS). The wavelength of the incidence X-rays was selected at 0.180 nm with an energy resolution of 1.5 % by a multilayer monochromator. The diffraction pattern was monitored through a linear detector having an angular range of 14° in 2θ. These diffractograms are plotted as a function of temperature and diffraction angle using a linear gray-scale map for the recorded intensities, where darker represents a higher intensity.

Further identification of the formed phases is enabled through *ex situ* X-ray pole figures, measured for samples quenched at 700 °C. For recording such pole figures, the sample is tilted around both the in-plane and out-of-plane axes (denoted as the χ and ϕ angle, respectively), to obtain information on the preferential orientation of the probed crystalline planes. A polar plot of the diffraction intensity then represents the distribution of the crystalline plane's preferred orientation, also denoted as the *texture* of the crystal grains. The pole figures reported in this work were acquired using a four-circle diffractometer at the X20A beamline of the NSLS, using X-rays with a wavelength of $\lambda =$

0.154 nm, and a custom linear detector covering 20 to 60° in 2θ, and by scanning the sample in χ and ϕ in steps of 1°. The pole figures of the thinnest samples, i.e. an as-deposited Ni thickness of 3 nm, were acquired with a double acquisition time, to ensure that adequate intensities could be collected. The pole figures are displayed using a grayscale map for the recorded intensities (with black corresponding to the highest intensity). They are aligned so the Si substrates are oriented in the same direction, as depicted in the supplementary material. A ring of higher intensity was observed at $\chi \sim 60°$ and is present in most of the acquired pole figures, including a measurement of a Si reference sample, indicating that this is related to background. Further details concerning the set-up used for these pole-figure measurements can be found in our earlier work [15, 16]. The extensive literature available on silicide and germanide textures was recently reviewed by De Schutter *et al.* [17].

Bright field transmission electron microscopy (BF-TEM) overview images were acquired by using a FEI-Tecnai electron microscope operated at 200kV. Scanning transmission electron microscopy energy dispersive X-ray spectroscopy (STEM-EDS) measurements were made using a FEI-Osiris electron microscope operated at 200kV, equipped with a ChemiSTEM system [18]. For the acquisition and quantification of the maps, the ESPRIT software was used.

3. Results

The unalloyed Ni thickness library was first investigated *ex situ* after applying an anneal to 700 °C. After the temperature treatment, visual inspection of the gradient indicates an abrupt boundary between two regions in the thickness library with a clear difference in color. This boundary is situated at a thickness of t_c= 4.8 nm (Fig. 1b) and SEM images in figure 1c show that the color change is due to a different morphology of the sample. Films thicker than t_c showed agglomerated grains and those thinner than t_c were almost feature-less (Fig. 1).

In situ XRD confirms that the observed critical boundary t_c is the demarcation line between the two thickness regimes that are described in the literature

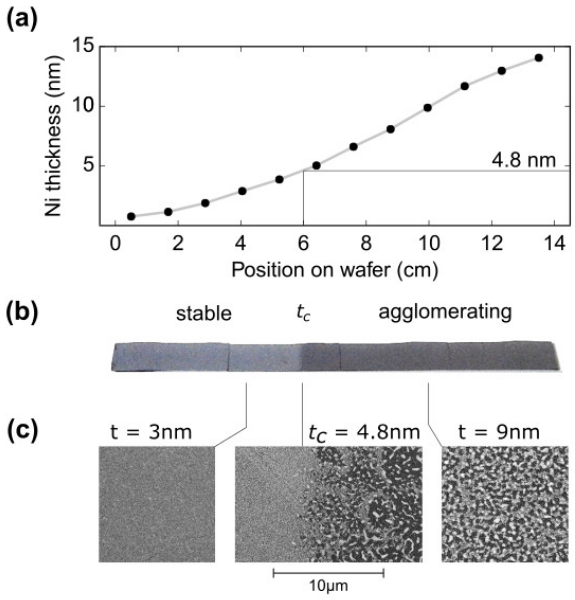

Figure 1: Thickness gradients were used to study the solid-state reaction between Ni and Si(001). **(a)** The equivalent Ni thickness was determined from RBS measurements, showing a quasi-linear dependence of de thickness with the position on the wafer. **(b)** Photographic picture of a 150 mm long strip from the thickness gradient after annealing to 700 °C, exhibiting a clear color change at a Ni thickness of t_c= 4.8 nm. **(c)** SEM micrographs conducted at several positions on the annealed gradient show a significant difference in morphology at t_c.

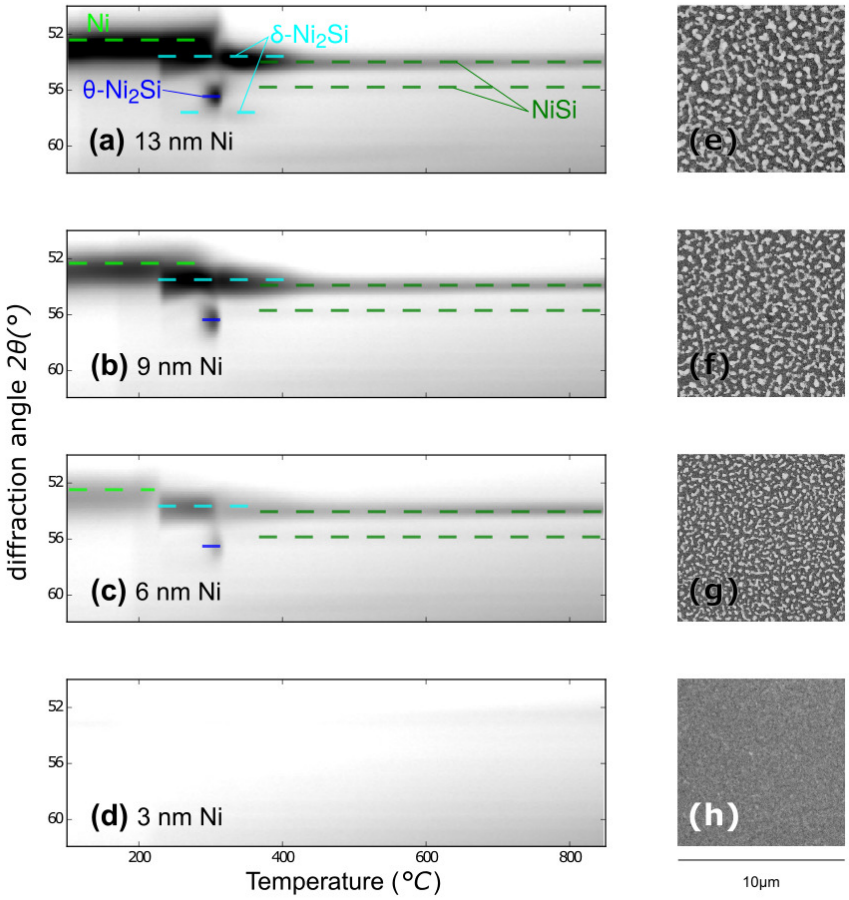

Figure 2: *In situ* XRD measurements during annealing indicate a significant difference in phase formation above and below the critical thickness t_c= 4.8 nm. The sequence of several silicides is observed for films thicker than t_c, whereas thinner films do not show any diffraction, indicating the possible formation of epitaxial silicides.

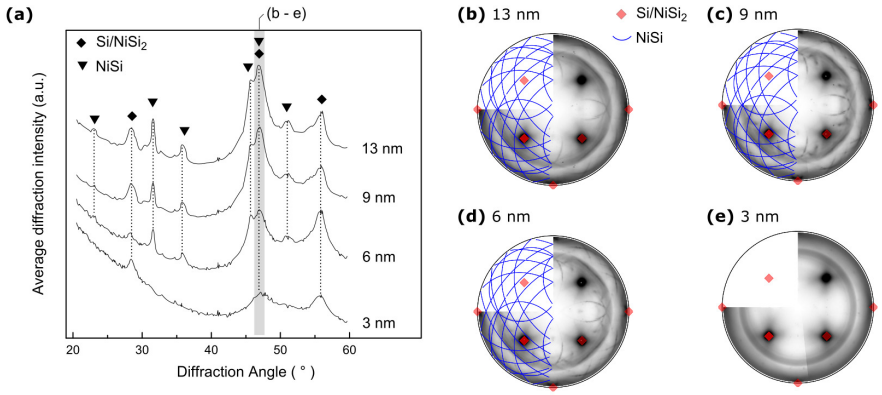

Figure 3: **(a)** Pole figures acquired from Ni samples quenched at 700 °C integrated in χ and ϕ result in a powder-like diffraction pattern, allowing unambiguous phase identification. Further investigation of the individual pole figure at $2\theta \simeq 47.5^{\circ}$ (covering diffraction of NiSi(211)/(202) and $NiSi_2$(202) planes) shows the axiotaxial texture of the NiSi phase for 13 **(b)**, 9 **(c)** and 6 nm **(d)** Ni. 3 nm **(e)** Ni instead only contains features originating from either the Si substrate and/or type-A epitaxial $NiSi_2$.

[9, 10, 11]. Indeed, samples above the critical thickness (e.g. 6, 9 and 13 nm, Fig. 2a, b and c) show the well-known phase sequence which forms NiSi above 400 °C, after first forming intermediate δ-Ni_2Si and transient θ-Ni_2Si [19]. However, *in situ* XRD from samples below the critical thickness (e.g. 3 nm, Fig. 2d) do not show any clear diffraction signal from silicide phases formed during the anneal. We equate the absence of diffraction to the formation of epitaxial silicides. Due to the fixed geometry of the *in situ* XRD set-up, diffracting planes will only be observed if they are oriented (nearly) parallel to the substrate's surface. Consequently, an epitaxial phase does not necessarily diffract in the probed reciprocal space.

The sudden change in phase formation at the critical thickness is further corroborated by *ex situ* pole-figure measurements. Within these measurements, diffraction intensities are monitored while the sample is rotated both in- and out-of-plane (respectively angles ϕ and χ), thus avoiding the issues related with a fixed geometry described above. As a first step in the pole-figure data analysis, one can use these measurements for unambiguous phase identification by

integrating the observed intensity over all ϕ and χ, for every value of 2θ. This approach results in a diffraction pattern that includes diffraction of all planes, independently of their geometrical orientation in respect to the samples' surface. Such 'powder-like' diffraction patterns are displayed in Fig. 3. Samples above the critical thickness clearly include diffraction from both the Si-substrate and the NiSi silicide, whereas samples below the critical thickness only contain higher intensity near $2\theta \sim 28.5^{\circ}$, 47.5° and 56.4°, corresponding to diffraction of either the Si substrate or $NiSi_2$, whose diffraction angles coincide due to a similar crystal lattice.

Our second step to analyse the pole-figure data is by displaying the diffraction intensities as a function of polar χ and ϕ angles for a fixed diffraction angle. Inspecting the individual pole figures at the interesting diffraction angles, such as those displayed in figures 3b-e, further corroborates the above observations. The presence of NiSi for thicker films is evidenced by the circular features on the pole figures, indicating a poly crystalline NiSi layer with axiotaxial texture. Below the critical thickness, no silicide diffraction can be observed. However, from the literature, we expect that epitaxial $NiSi_2$ is formed below the critical thickness. Due to the very similar face-centered cubic lattices of $NiSi_2$ and the Si substrate, with only 0.46 % difference in lattice parameter, the $NiSi_2$ grains can epitaxially align with the substrate, resulting in an overlap in pole-figure diffraction at the same χ, ϕ and 2θ angles as the Si substrate. This specific alignment, which is called *type-A* epitaxy, has been observed previously in the literature for these thin films [8, 9]. Pole figures are not able to distinguish the diffraction between the Si substrate and the $NiSi_2$ film, as the former saturates the detector due to high diffraction intensities. These pole-figure measurement exclude the presence of any other silicide except type-A oriented $NiSi_2$ below the critical thickness at this temperature. The occurrence of type-A epitaxial $NiSi_2$ at these as-deposited Ni thicknesses is in confirmation with the literature [8, 9, 10, 11]

The observation of such a clear thickness-dependent effect through the use of combinatorial libraries illustrates the unique capability of these thickness

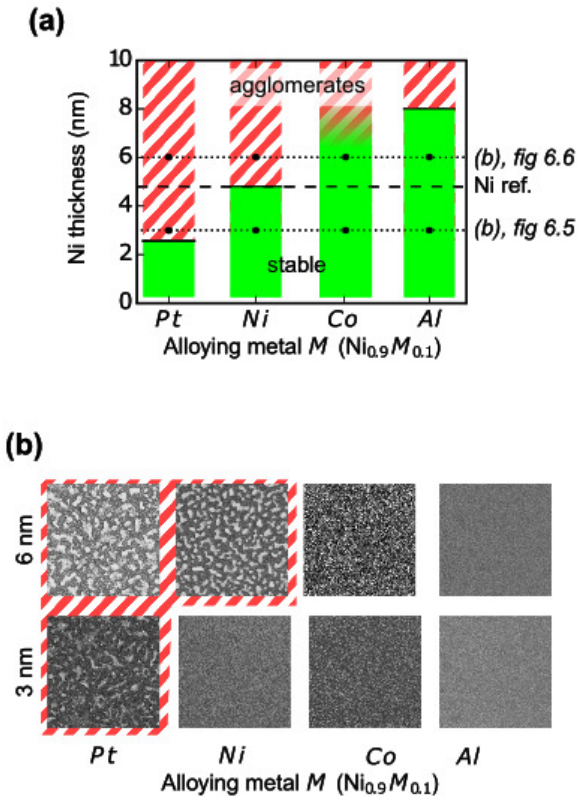

Figure 4: Unalloyed and alloyed (10 at.% Al, Co and Pt) thickness gradients were quenched at 700 °C in order to determine the critical thickness differences in morphological stability. Co-alloying shows a continuous increase in roughness as a function of Ni thickness.

gradients to investigate the critical thickness in the Ni-Si solid-state reaction as a function of position.

3.1. Effect of alloying on the critical thickness

Thickness gradients were subsequently used to investigate the critical change in phase formation when ternary elements are included in the as-deposited layer. Thickness gradients, alloyed with 10 at.% Al, Co or Pt, were again quenched at 700 °C. Samples with Al or Pt show a similar critical change in morphology at positions equivalent to a Ni thickness of $t_c = 8.0$ and 2.6 nm, respectively (Fig. 4). The changes in equivalent thickness is not the consequence of a merely

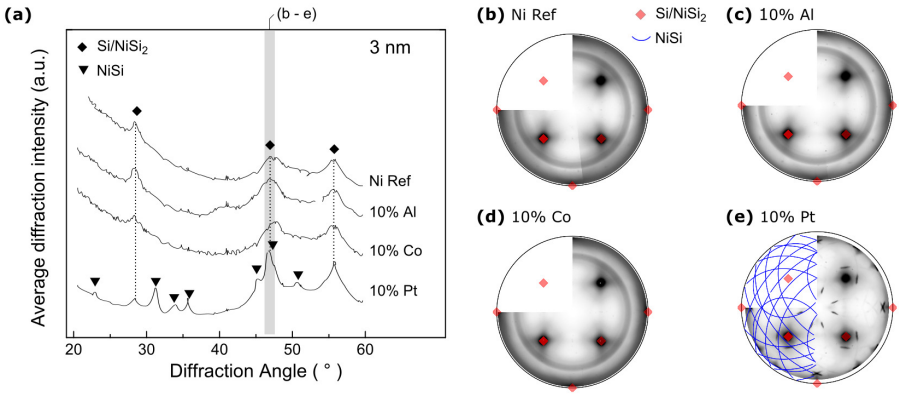

Figure 5: **(a)** The constructed powder-like diffraction patterns are used to identify the formed silicde after annealing 3 nm thick Ni films, which are alloyed with 10 at.% Al, Co or Pt, to 700 °C. The individual pole figures at $2\theta \simeq 47.5°$ exclude the occurence of any other silicide phase except type-A epitaxial $NiSi_2$ being formed for an unalloyed Ni film **(b)**, or when alloyed with Al **(c)** or Co **(d)**. NiSi is clearly present when alloyed with Pt **(e)**.

increased metal supply, e.g. the combination of 2.6 nm Ni in addition to 10 at.% Pt) is far less than the critical thickness $t_c = 4.8$ nm for unalloyed Ni films. When the gradient strip was alloyed with Co, no visual abrupt difference in morphology was observed as a function of thickness. SEM images (not shown) instead show an increased roughness for Ni thicknesses between 5 and 11 nm, but do not show the severe agglomeration as observed for an unalloyed film.

Further investigation of these alloyed thickness gradients through *ex situ* pole figures confirms that the value of t_c can indeed be varied through alloying. A selection of these measurements is displayed for 3 and 6 nm as-deposited Ni thickness in figures 5 and 6, respectively. The simulated 'powder-like' diffraction patterns (5a and 6a) includes diffraction intensities regardless of the diffraction plane's orientation, and unambiguously allows the identification of the crystalline phases present in the film. When 3 nm films are alloyed with Al or Co, no significant differences are observed by comparing these measurements with those of an unalloyed Ni film. However, Pt alloyed samples now clearly contain NiSi diffraction.

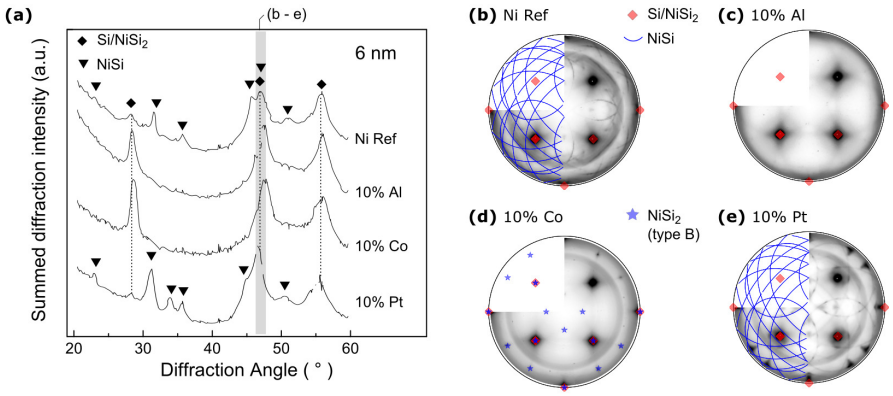

Figure 6: **(a)** The constructed powder-like diffraction patterns are used to identify the formed silicde after annealing 6 nm thick Ni films, which are alloyed with 10 at.% Al, Co or Pt, to 700 °C. NiSi is clearly present for the unalloyed film **(b)**, or when Pt is used as ternary element **(e)**. The individual pole figures at $2\theta \simeq 47.5^{\circ}$ confirm the absence of any silicide other than $NiSi_2$ when 10 at.% Al or Co are added.

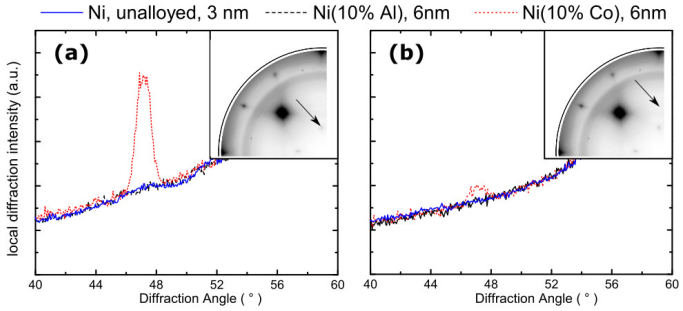

Figure 7: The diffraction intensities of a selection of samples for two specific orientations: (a) $\phi = 90^{\circ}$, and $\chi = 90^{\circ}$, corresponding with type-B oriented $NiSi_2(220)$ planes ($2\theta = 47.3^{\circ}$), and (b) $\phi = 90^{\circ}$, and $\chi = 32^{\circ}$, corresponding with randomly-oriented $NiSi_2(220)$ planes ($2\theta = 47.3^{\circ}$). The insets illustrate the location of these coordinates on the $NiSi_2(220)$ polefigure of the Co-alloyed sample.

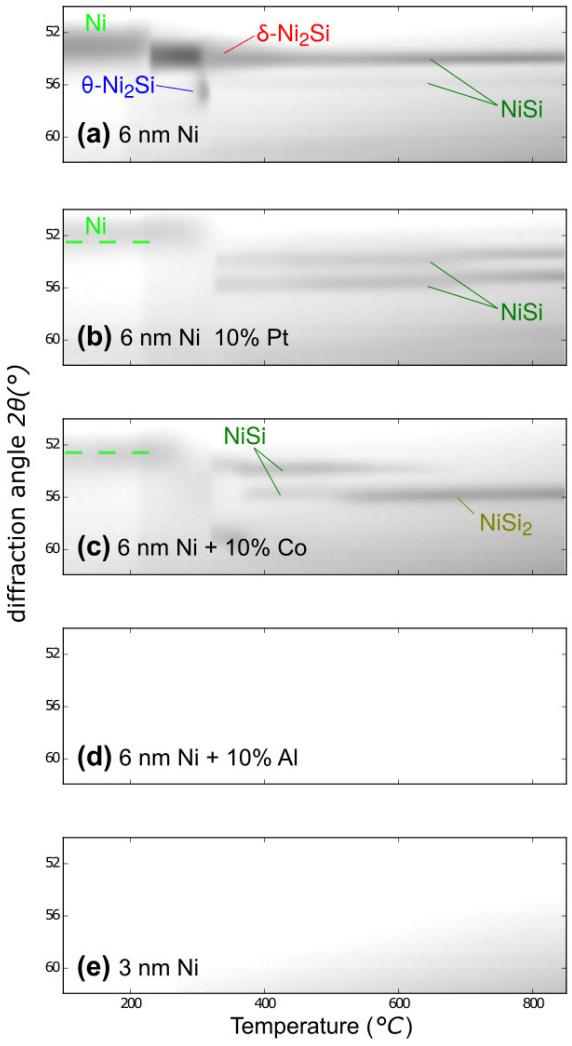

Figure 8: *In situ* XRD measurements of 6 nm thick Ni films during annealing indicate a significant difference in phase formation when comparing an unalloyed film **(a)** with a Pt **(b)**, Co **(c)** or Al-alloyed **(d)** film. The latter sample shows no recognisable diffraction patterns, and as such is comparable with an unalloyed 3 nm Ni film **(e)**.

Films with a slightly higher equivalent Ni thickness, e.g. 6 nm, are also significantly influenced through alloying (Fig. 6). Although NiSi was observed for an unalloyed film to form at this thickness, no such diffraction patterns are observed when Ni was alloyed with either Co or Al. No other silicide diffraction can be observed except $NiSi_2$, a clear indication that Co and Al alloying favours the low-temperature phase formation of $NiSi_2$. Closer inspection of the pole figures reveals an intriguing difference in $NiSi_2$ texture. Indeed, the sample containing 10 at.% Co now clearly contains diffraction of epitaxial $NiSi_2$ identified as the *type-B* orientation. This epitaxial orientation is characterised by diffraction spots on the displayed pole figures, and can be related to type-A $NiSi_2$ epitaxy through a rotation of 180° around the {111} direction. Furthermore, randomly-oriented $NiSi_2$ grains are evident when alloying with Co from an overall increase in $NiSi_2$-diffraction intensity at χ and ϕ angles unrelated to type A or type B epitaxy. This is illustrated in figure 7, which displays the diffraction intensities at specific locations within the reciprocal space (in contrast to the patterns displayed in Figures 3 and 6, which were integrated over all measured χ and ϕ angles). Figure 7a corresponds with type-B oriented grains, and Figure 7b corresponds with randomly-oriented grains, both of which are only present in the Co-alloyed sample. Pole-figure measurement do not allow to estimate which fraction of the silicide is randomly-aligned, or along a type-A or B epitaxy. Al-alloying does not include the type-B features and therefore the pole figures exclude type-B epitaxy. Furthermore, these samples do not contain diffraction related to randomly-oriented $NiSi_2$, suggesting that only type-A $NiSi_2$ is present, similar to the case of an unalloyed Ni film thinner than t_c.

Although Al and Co clearly favour the low-temperature formation of $NiSi_2$, these observations at 700 °C do not guarantee that the silicide phase formation is identical to the ultrathin phase sequence, as low-temperature NiSi can still be formed prior to the formation of $NiSi_2$. This question is answered through the *in situ* XRD measurements for 6 nm thick samples, as displayed in figure 8. From these measurements, we observe that the silicide phase sequence still includes NiSi at low temperatures when Co is used as alloy, while no NiSi is observed for

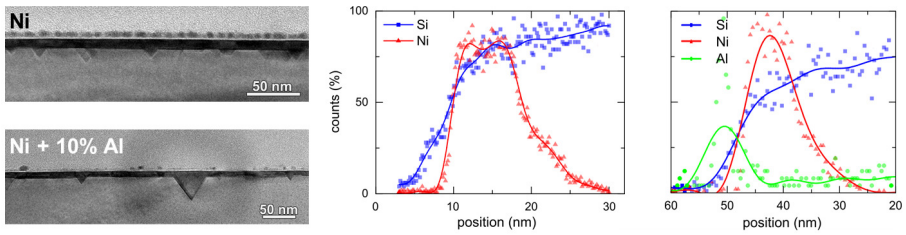

Figure 9: **(left)** BF-TEM images show the interface roughness of 3 nm Ni films without alloying, and of 6 nm Ni films with Al alloying. The EDS line scans **(right)** show the distribution of the alloying atoms throughout the layer thickness.

the Al-alloyed sample. We thus conclude that the critical thickness is not shifted to higher values by Co-alloying, as the phase sequence is not drastically altered and instead the transformation temperature of NiSi to $NiSi_2$ is significantly reduced. On the other hand, Al alloying lacks all diffraction peaks through the full temperature anneal, similar to the solid-state reaction as observed for unalloyed Ni films below t_c and indicating a promotion of the ultrathin phase sequence to thicker films. We thus conclude that the critical thickness t_c can indeed be changed by alloying, both to higher values (Al), as well as to lower values (Pt). Although Co-alloying does promote low-temperature formation of $NiSi_2$, it does not change the phase sequence above the original value of t_c.

In order to evaluate the final distribution of the ternary elements, a sample of 3 nm unalloyed Ni, below the critical thickness, and an Al-alloyed sample of 6 nm Ni , were studied through TEM-imaging after quenching (Fig. 9). The unalloyed sample shows atomically-sharp interfaces along both the Si{100} and Si{111} directions. The latter creates triangular facets, which submerge deep into the Si substrate. Al alloying does not change this image, although Allenstein *et al.* report that the typical {111} faceting disappears when alloying 20 nm Ni films with higher Al concentrations (i.e. > 20 at.%) [20]. More interesting, however, is the positioning of the alloying species throughout the silicide as determined through EDS-mapping, where almost all Al remains largely on the surface.

4. Discussion

The critical change in phase formation in these ultra-thin films is indicative of the competitive behaviour in the low-temperature formation of either NiSi and $NiSi_2$ [21]. The energetic threshold for atoms to nucleate into either of these phases can be described to be proportional to $\Delta\sigma^3/(\Delta H - T\Delta S)^2$, with $\Delta\sigma$, ΔH and ΔS representing the differences in interface energy, enthalpy and entropy due to the nucleation, respectively. The enthalpy of formation of the nickel silicides are comparable with one-another [19] $\delta - Ni_2Si$: -46.9, $NiSi$: -42.4, $NiSi_2$: 29.3 kJ/mol of atoms [22]. As such, effects that change the interface energy and entropy have the potential to significantly alter the phase stability and solid-phase reaction. One can use the above equation as a framework to interpret and qualitatively rationalize the effect of ternary elements on the phase formation through entropy-considerations.

An alloy which is soluble in the forming phase will increase that phases' entropy, whereas an insoluble alloy will instead require that it should be excreted before the silicide can be formed. By consequence, soluble alloys will decrease the energy threshold for silicide nucleation whereas insoluble alloys will increase the threshold due to the required atomic transport. This argument has been used in the past to understand observed changes in ternary silicide formation for thicker films [23, 24, 25, 26, 27, 28, 29]. We can thus categorise the three used alloys in three different classes, according to their solubility in NiSi or $NiSi_2$. According to high-temperature ($> 800\,^{\circ}\mathrm{C}$) equilibrium ternary phase diagrams, $NiSi_2$ allows relatively high incorporation of Al and Co atoms (20 at.% for Al [30], and complete miscibility of Co instead of Ni [31]), but not of Pt. Pt is highly soluble in NiSi, whereas the solubility of Al and Co is limited to respectively 1.5 [30] and 10 % [31]. On the basis of the above, one then expects Pt to promote the formation of NiSi but to delay the formation of $NiSi_2$, and vice versa for Al. Co, however, is reasonably soluble in both phases, although to different extents. We therefore speculate that Co will not hinder the initial nucleation of NiSi grains, and so does not shift the critical thickness. However, it will

significantly lower the nucleation temperature of $NiSi_2$, similar to the discussion of Lavoie *et al.* [25] and Smeets *et al.* [32], so $NiSi_2$ is formed before NiSi can severely agglomerate, resulting in a non-agglomerated film after annealing to 700 °C, as observed from the morphology evaluation of the gradient shown in figure 4. We want to point out to the reader that experiments with a higher Co concentration of 25 at.% has been reported to increase the critical thickness [33], promoting the formation of $Ni_xCo_{1-x}Si_2$ without first forming a mono-silicide. This difference with our experiments indicates that the influence of Co on the nickel silicide formation is different when one adds more Co to the initial film than the solubility limit of Co within NiSi (e.g. 10 at.%). Several studies on the effect of alloying elements with higher alloying concentrations also include the formation of other phases such as CoSi [34] or NiAl [20], but where not observed in our *in situ* XRD measurements or our pole-figure XRD measurements. Our experiments with 10 at.% Ge and Pd alloying at discrete Ni thicknesses (i.e. 2, 3, 6 and 9 nm) indicate that the value of the critical thickness has decreased to below t_c= 3 nm. These data are attached to this paper as supplementary information but are not further discussed in the body of this paper. As Ge and Pd have similar solubility properties as Pt, these experiments corroborate the solubility argument for explaining the effect of alloying on the phase formation.

Luo *et al.* argued that the drastically altered silicide phase sequence as a function of thickness is related to the silicide-silicon interface. The energy required to facilitate this interface will become increasingly important in the total energy balance when going to thinner films. Therefore, epitaxial $NiSi_2$ is expected to be favoured on a non-epitaxial phase such as NiSi. One can argue that the interfacial energy of the silicide-silicon interface will also be influenced through alloying. Discussions based on interface energy are not straightforward, due to a lack on experimental data on the interface energy. More recently, Kousseifi *et al*[35] could quantitatively determine the interface energy for Pt-alloyed NiSi and θ-Ni_2Si. However, different alloys, or different alloying concentration, can alter the preferential orientation of silicides or change the interface energy through accumulation at the grain-boundaries. As a consequence, we do not

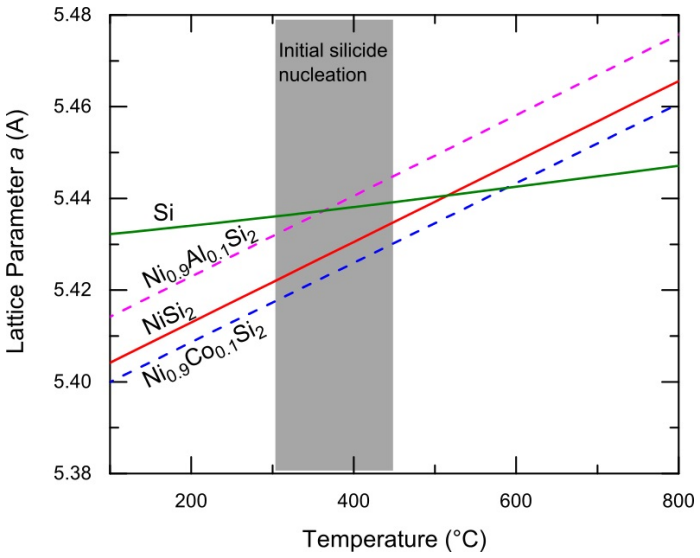

Figure 10: Evolution of the lattice parameters of Si and $NiSi_2$. The influence of the alloyed elements was estimated based upon their room-temperature lattice parameter and by assuming a similar coefficient of thermal expansion.

have access to the necessary information to evaluate the effect of the interface energy on the energetic competation between NiSi- or $NiSi_2$-formation. Further study that focuses on the interface, and the interphase-interface energy should prove valuable to the field. Nevertheless, we rely on the interface-energy to discuss the significant increase in randomly-aligned $NiSi_2$ grains upon Co-alloying (Figure 7). In the ultra-thin phase formation regime, the formation of epitaxial type-A $NiSi_2$ requires an almost perfect lattice match across the interface during initial nucleation and subsequent growth. Such a crystal match is indeed possible due to the same crystal lattice and similar lattice parameter between $NiSi_2$ and the Si substrate. The lattice constant of $NiSi_2$ differs only 0.46% at room temperature, and due to the different thermal expansion coefficients ($\alpha = 16.25 \times 10^{-6}\,\mathrm{K}^{-1}$ for $NiSi_2$ [36] and $\alpha = 2.55 \times 10^{-6}\,\mathrm{K}^{-1}$ for Si [37]), an exact lattice match is expected during the heating process around 520 °C (Fig. 10). However, due to the smaller lattice parameter of $CoSi_2$, a delay in lattice-match is expected during the heating process when using Co as an alloying element.

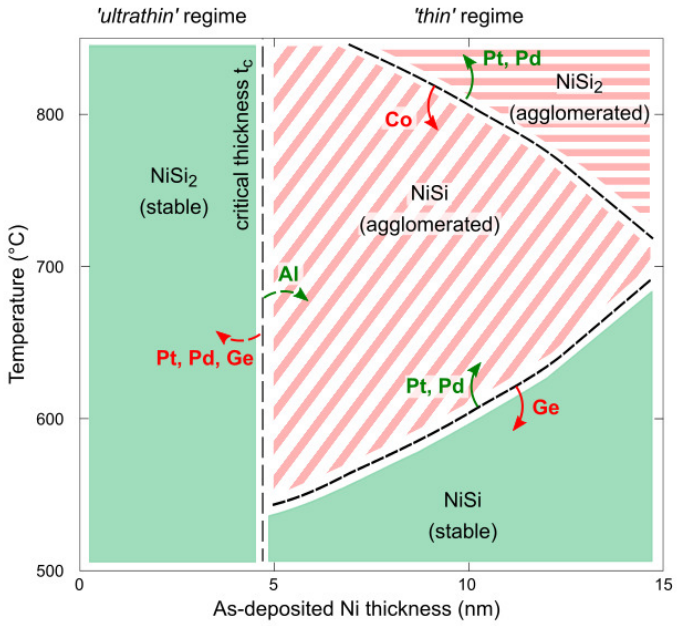

Figure 11: Overview of the thermodynamic and morphological stable regimes for nickel silicides as a function of thickness and annealing temperature. Alloying the initial Ni film with low ($< 10\%$) concentration of Al, Co, Ge, Pd, Pt are known to influence these degradation temperatures.

On the other hand, Al is reported to increase the lattice parameter of $NiSi_2$, and as such, lowers the temperature at which we expect an exact lattice match. From *in situ* sheet resistance data [9], we expect the initial nucleation of $NiSi_2$ grains in the ultrathin phase formation regime between 300-400 °C. By consequence, we propose that Al-alloying will require less strain or interfacial defects at nucleation to compensate the difference in the lattice parameter than Co-alloying. In other words, on the basis of lattice matching arguments one would also conclude that alloying with Al is expected to lower the energy threshold to form epitaxial $NiSi_2$ at low temperatures.

Our results can be put into the broader context of stable nickel silicide contacts. The degradation of nickel silicides is discussed ever since NiSi was first considered as a contact material for the transistors' source and drain regions.

The stability of a NiSi film is challenged through (1) agglomeration and (2) nucleation into $NiSi_2$. For 'ultrathin' (< 5 nm) Ni films, the agglomerating NiSi phase is not formed and instead $NiSi_2$ was found to be stable (both morphologically as well as thermodynamically) up to 900 °C. Figure 11 shows a diagram to indicate the temperature and thickness regions at which a stable nickel silicide is present. Three borders limit the formation of a stable silicide compound: the critical thickness t_c, the agglomeration temperature of NiSi and the nucleation temperature of NiSi into $NiSi_2$. The agglomeration temperature decreases with decreasing film thickness, which can be explained as a thinner film has a higher surface-to-volume ratio [9]. The nucleation temperature of NiSi to $NiSi_2$ was studied by Deduytsche *et al.* [3] and is observed to increase for decreasing Ni thickness. Therefore, agglomeration is the most important degeneration mechanism for these thin-film silicides. Alloying proves a valuable strategy to alter positions of these three borders as a function of thickness and temperature, and numerous publications have previously elaborated on the beneficial effect of alloys on NiSi stability. We note to the reader that the literature also reports on beneficial effects of alloying elements not included in this study, such as Mo [38], Ti[39], Ta[40] or W[40, 38]. Their effect on the critical thickness has not yet been evaluated. Figure 11 displays the shifts through alloying for those alloying species which are relevant to this article: Al, Co [25, 41, 32], Ge [42, 43], Pd [25] and Pt [5]. Our study represents a systematic investigation of several alloying elements on the critical thickness t_c.

5. Conclusions

The Ni-Si solid-state reaction was studied in the sub-15 nm Ni thickness regime. The morphological stability of the formed silicides indicates a critical thickness $t_c = 4.8$ nm that separates the '*regular*' phase sequence, which forms agglomerating NiSi, from the more stable '*ultrathin*' phase sequence, which forms epitaxial $NiSi_2$ at low temperatures. Thickness gradient libraries were fabricated to investigate the effect of ternary elements (10 at.% Al, Co and Pt) on the value

of t_c as a function of thickness in a semi-continuous fashion. We found that t_c can be increased or decreased at will, by the addition of Al (t_c= 8.0 nm) and Pt (t_c= 2.6 nm) as alloy. Co did not change the phase sequence, did not display an abrupt critical thickness. It did, however, alter the transformation temperature of NiSi into $NiSi_2$ which resulted in a rough but non-agglomerating silicide film. Several energetic parameters are discussed to understand the observed shift in relation to mixing entropy and interface energy. This study shows that the solid-phase reaction of silicides exhibits drastic non-linear behaviour upon thickness scaling, and which can be influenced and controlled by altering the as-deposited composition.

Supplementary Materials

All polefigures displayed in this article are oriented with fixed position in reference to the Si substrate, as displayed in the supplementary material online.

Overview of *in situ* XRD measurements and SEM micrographs of 10 nm Ni, alloyed with 10 at.% Ge and Pd are also displayed in the supplementary material.

Acknowledgement

The authors acknowledge the FWO Vlaanderen, the Hercules foundation and BOF-UGent (GOA 01G01513) for providing financial support for this work. This research used resources of the National Synchrotron Light Source, a U.S. Department of Energy (DOE) Office of Science User Facility operated for the DOE Office of Science by Brookhaven National Laboratory under Contract No. DE-AC02-98CH10886.

References

[1] C. Lavoie, F. d'Heurle, C. Detavernier, C. Cabral, Towards implementation of a nickel silicide process for CMOS technologies, Microelectronic Engineering 70 (2) (2003) 144–157.

[2] A. Lauwers, J. A. Kittl, M. J. Van Dal, O. Chamirian, M. A. Pawlak, M. de Potter, R. Lindsay, T. Raymakers, X. Pages, B. Mebarki, et al., Ni based silicides for 45nm CMOS and beyond, Materials Science and Engineering: B 114 (2004) 29–41.

[3] D. Deduytsche, C. Detavernier, R. Van Meirhaeghe, C. Lavoie, High-temperature degradation of NiSi films: Agglomeration versus $NiSi_2$ nucleation, Journal of Applied Physics 98 (3) (2005) 033526.

[4] J. Kittl, K. Opsomer, C. Torregiani, C. Demeurisse, S. Mertens, D. Brunco, M. Van Dal, A. Lauwers, Silicides and germanides for nano-CMOS applications, Materials Science and Engineering: B 154 (2008) 144–154.

[5] D. Mangelinck, J. Dai, J. Pan, S. Lahiri, Enhancement of thermal stability of NiSi films on (100) Si and (111) Si by Pt addition, Applied Physics Letters 75 (12) (1999) 1736–1738.

[6] Z. Zhang, S. Zhang, B. Yang, Y. Zhu, S. M. Rossnagel, S. Gaudet, A. J. Kellock, J. Jordan-Sweet, C. Lavoie, Morphological stability and specific resistivity of sub-10 nm silicide films of Ni Pt_x on Si substrate, Applied Physics Letters 96 (2010) 071915.

[7] N. Breil, C. Lavoie, A. Ozcan, F. Baumann, N. Klymko, K. Nummy, B. Sun, J. Jordan-Sweet, J. Yu, F. Zhu, et al., Challenges of nickel silicidation in CMOS technologies, Microelectronic Engineering 137 (2015) 79–87.

[8] R. Tung, J. Poate, J. Bean, J. Gibson, D. Jacobson, Epitaxial silicides, Thin Solid Films 93 (1) (1982) 77–90.

[9] K. De Keyser, C. Van Bockstael, R. Van Meirhaeghe, C. Detavernier, E. Verleysen, H. Bender, W. Vandervorst, J. Jordan-Sweet, C. Lavoie, Phase formation and thermal stability of ultrathin nickel-silicides on Si (100), Applied Physics Letters 96 (17) (2010) 173503.

[10] Z. Zhang, B. Yang, Y. Zhu, S. Gaudet, S. Rossnagel, A. J. Kellock, A. Ozcan, C. Murray, P. Desjardins, S. Zhang, et al., Exploitation of a self-

limiting process for reproducible formation of ultrathin $Ni_{1-x}Pt_x$ silicide films, Applied Physics Letters 97 (25) (2010) 252108.

[11] J. Fouet, M. Texier, M.-I. Richard, A. Portavoce, D. Mangelinck, C. Guichet, N. Boudet, O. Thomas, Silicide formation during reaction between Ni ultra-thin films and Si (001) substrates, Materials Letters 116 (2014) 139–142.

[12] L. Knoll, Q. Zhao, S. Habicht, C. Urban, B. Ghyselen, S. Mantl, Ultrathin Ni silicides with low contact resistance on strained and unstrained silicon, IEEE Electron Device Letters 31 (4) (2010) 350–352.

[13] L. Knoll, Q. Zhao, R. Luptak, S. Trellenkamp, K. Bourdelle, S. Mantl, 20nm Gate length Schottky MOSFETs with ultra-thin NiSi/epitaxial $NiSi_2$ source/drain, Solid-State Electronics 71 (2012) 88–92.

[14] X. Gao, J. Andersson, T. Kubart, T. Nyberg, U. Smith, J. Lu, L. Hultman, A. J. Kellock, A. Zhang, C. Lavoie, et al., Epitaxy of ultrathin $NiSi_2$ films with predetermined thickness, Electrochemical and Solid-State Letters 14 (7) (2011) H268–H270.

[15] C. Detavernier, J. Jordan-Sweet, C. Lavoie, Texture of NiSi films on Si (001),(111), and (110) substrates, Journal of Applied Physics 103 (11) (2008) 113526.

[16] B. De Schutter, K. De Keyser, C. Detavernier, Visualization and classification of epitaxial alignment at hetero-phase boundaries, Thin Solid Films 599 (2016) 104–112.

[17] B. De Schutter, K. De Keyser, C. Lavoie, C. Detavernier, Texture in thin film silicides and germanides: A review, Applied Physics Reviews 3 (3) (2016) 031302.

[18] P. Schlossmacher, D. Klenov, B. Freitag, H. Von Harrach, Enhanced detection sensitivity with a new windowless XEDS system for AEM based on silicon drift detector technology, Microscopy Today 18 (04) (2010) 14–20.

[19] S. Gaudet, C. Coia, P. Desjardins, C. Lavoie, Metastable phase formation during the reaction of Ni films with Si (001): The role of texture inheritance, Journal of Applied Physics 107 (9) (2010) 093515.

[20] F. Allenstein, L. Budzinski, D. Hirsch, A. Mogilatenko, G. Beddies, R. Grötzschel, H. Hinneberg, Influence of Al on the growth of $NiSi_2$ on Si (001), Microelectronic Engineering 82 (3) (2005) 474–478.

[21] J. Luo, Z. Qiu, C. Zha, Z. Zhang, D. Wu, J. Lu, J. Åkerman, M. Östling, L. Hultman, S. Zhang, Surface-energy triggered phase formation and epitaxy in nanometer-thick $Ni_{1-x}Pt_x$ silicide films, Applied Physics Letters 96 (3).

[22] M. E. Schlesinger, Thermodynamics of solid transition-metal silicides, Chemical Reviews 90 (4) (1990) 607–628.

[23] C. Detavernier, R. Van Meirhaeghe, F. Cardon, K. Maex, Influence of mixing entropy on the nucleation of $CoSi_2$, Physical Review B 62 (18) (2000) 12045.

[24] A. Lauwers, M. De Potter, O. Chamirian, R. Lindsay, C. Demeurisse, C. Vrancken, K. Maex, Silicides for the 100-nm node and beyond: Co-silicide, Co (Ni)-silicide and Ni-silicide, Microelectronic Engineering 64 (1) (2002) 131–142.

[25] C. Lavoie, C. Detavernier, C. Cabral, F. dHeurle, A. Kellock, J. Jordan-Sweet, J. Harper, Effects of additive elements on the phase formation and morphological stability of nickel monosilicide films, Microelectronic Engineering 83 (11) (2006) 2042–2054.

[26] J. Demeulemeester, D. Smeets, C. Comrie, N. Barradas, A. Vieira, C. Van Bockstael, C. Detavernier, K. Temst, A. Vantomme, On the growth kinetics of Ni (Pt) silicide thin films, Journal of Applied Physics 113 (16) (2013) 163504.

[27] J. Toinin, A. Portavoce, M. Texier, M. Bertoglio, K. Hoummada, First stages of Pd/Ge reaction: Mixing effects and dominant diffusing species, Microelectronic Engineering.

[28] A. Schrauwen, J. Demeulemeester, D. Deduytsche, W. Devulder, C. Detavernier, C. Comrie, K. Temst, A. Vantomme, Ternary silicide formation from Ni-Pt, Ni-Pd and Pt-Pd alloys on Si (100): Nucleation and solid solubility of the monosilicides, Acta Materialia 130 (2017) 19–27.

[29] A. Schrauwen, K. Van Stiphout, J. Demeulemeester, B. De Schutter, W. Devulder, C. Comrie, C. Detavernier, K. Temst, A. Vantomme, The role of composition and microstructure in Ni-W silicide formation and low temperature epitaxial $NiSi_2$ growth by premixing Si, Journal of Physics D: Applied Physics 50 (6) (2017) 065303.

[30] K. Richter, K. Chandrasekaran, H. Ipser, The Al–Ni–Si phase diagram. Part II: phase equilibria between 33.3 and 66.7 at.% Ni, Intermetallics 12 (5) (2004) 545–554.

[31] J. Van Beek, P. Oberndorff, A. Kodentsov, F. Van Loo, Interactions in the Co–Ni–Si system at 800 C, Journal of Alloys and Compounds 297 (1) (2000) 137–143.

[32] D. Smeets, J. Demeulemeester, K. De Keyser, D. Deduytsche, C. Detavernier, C. Comrie, C. Theron, C. Lavoie, A. Vantomme, Nucleation and diffusion during growth of ternary Co1- xNixSi2 thin films studied by complementary techniques in real time, Journal of Applied Physics 104 (9) (2008) 093533.

[33] Z. Zhu, X. Gao, Y. Piao, C. Hu, Z. Qiu, Z.-B. Zhang, D. Wu, S.-L. Zhang, Phase formation and film morphology of ultrathin $co_{1-x}ni_xsi_2$ films, Journal of Vacuum Science & Technology A: Vacuum, Surfaces, and Films 30 (5) (2012) 050602.

[34] Y. Piao, Z. Zhu, X. Gao, A. Karabko, C. Hu, Z. Qiu, J. Luo, Z.-B. Zhang, S.-L. Zhang, D. Wu, Extensive raman spectroscopic investigation of ultrathin co1xnixsi2 films grown on si(100), Journal of Vacuum Science & Technology A: Vacuum, Surfaces, and Films 30 (4) (2012) 041511. doi:10.1116/1.4726295.

[35] M. El Kousseifi, K. Hoummada, T. Epicier, D. Mangelinck, Direct observation of NiSi lateral growth at the epitaxial θ-Ni_2 Si/Si (100) interface, Acta Materialia 99 (2015) 1–6.

[36] D. Smeets, G. Vanhoyland, J. D'Haen, A. Vantomme, On the thermal expansion coefficient of cosi2 and nisi2, Journal of Physics D: Applied Physics 42 (23) (2009) 235402.

[37] Y. Okada, Y. Tokumaru, Precise determination of lattice parameter and thermal expansion coefficient of silicon between 300 and 1500 k, Journal of Applied Physics 56 (2) (1984) 314–320.

[38] A. Derafa, G. Tellouche, K. Hoummada, A. Bouabellou, D. Mangelinck, Effect of alloying elements mo and w on ni silicides formation, Microelectronic Engineering 120 (2014) 150–156.

[39] Y. Setiawan, P. Lee, C. Tan, K. Pey, Effect of Ti alloying in nickel silicide formation, Thin Solid Films 504 (1) (2006) 153–156.

[40] D. Deduytsche, C. Detavernier, R. Van Meirhaeghe, J. Jordan-Sweet, C. Lavoie, Formation and morphological stability of NiSi in the presence of W, Ti, and Ta alloying elements, Journal of Applied Physics 101 (4) (2007) 044508.

[41] D. Deduytsche, C. Detavernier, R. Van Meirhaeghe, J. Jordan-Sweet, C. Lavoie, Formation and stability of NiSi in the presence of Co and Fe alloying elements, Journal of Vacuum Science & Technology B 26 (6) (2008) 1971–1977.

[42] T. Yang, G. Luo, E. Chang, T. Yang, H. Tseng, C. Chang, Study of nickel silicide contact on Si/Si_{1-x} Ge_x, IEEE Electron Device Letters 24 (9) (2003) 544–546.

[43] P. Besser, P. King, E. Paton, S. Robie, Ge effects on silicidation, Microelectronic Engineering 82 (3) (2005) 467–473.